APPLICATIONS OF SATELLITE MICROWAVE DATA FOR HURRICANE PREDICTIONS

TONG ZHU AND FUZHONG WENG

NOAA/NESDIS/Office of Research and Applications
5200 AuthRoad, Rm. 601, Camp Springs, MD 20746, USA
E-mail: tong.zhu@noaa.gov

(Manuscript received 6 January 2003)

The measurements obtained from satellite microwave sensors have been increasingly utilized in the numerical weather prediction models. In this study, we present a comprehensive method of using a variety of microwave products for the hurricane model initialization. Atmospheric temperature profiles are retrieved from the Advanced Microwave Sounding Unit (AMSU) and are then utilized to further derive the rotational winds for hurricane vortex by solving the nonlinear balance equation. In addition, the divergent winds associated with latent heat release are derived from the Omega equation based on the AMSU rain rate as a diabatic heating source. Atmospheric moisture profiles are iteratively retrieved from the AMSU derived total precipitable water (TPW). Furthermore, for hurricane simulations over oceans, the sea surface temperature (SST) is an important component in the overall hurricane initialization. This parameter can be uniquely derived from lower frequencies of satellite microwave sensors. The operational microwave SST products have been made available from the Tropical Rainfall Measuring Mission (TRMM) microwave imager (TMI).

The retrieved temperature, water vapor and wind fields associated with Hurricane Bonnie (1998) compare favorably to the dropsonde observations taken in the vicinity of the storm. Using these products as the model initial conditions, a 5-day explicit simulation of Hurricane Bonnie is performed and shows that the model can reproduces reasonably well the hurricane intensity changes and asymmetries in radar reflectivity. Trajectory analyses indicate that the upper-level westerly flow converges into the west eyewall, and then produces middle-level descend warming in the west to the south eyewall. The frontogenesis function is frontolytic in the west eyewall, with the contributions from deformation term at the low level and from tilting term at the middle and upper levels. It is shown that the upper-level strong westerly inflow is a key factor leading to the development of the partial eyewall.

1. Introduction

Tropical cyclones develop over the ocean, where few upper-air observations are available. The monitoring of tropical cyclones began with ship and commercial airline observations in the 1930s. Aircraft reconnaissance and radar observations were available in the 1940s. As compared with satellite observations, the above data have very limited area coverage. During the past three decades, many attempts have been made to incorporate satellite observations into hurricane models. The satellite retrieval products that were successfully incorporated and have potential use for hurricane models are: (a) visible and infrared channels observed winds, (b) microwave data retrieved rain rate, and (c) microwave data retrieved temperature. In the

following, we are going to give a brief review of these products and the methods to incorporate them into hurricane models.

The first Geostationary Operational Environmental Satellite (GOES) became available in June 1974. Today's geostationary satellites can detect visible imagery at 1-km spatial resolution and infrared imagery at 4-km spatial resolution at about 5-min intervals. The observed cloud patterns in such high temporal and spatial resolution provide a visualization of mesoscale meteorological processes. GOES satellites observations are extremely useful for determining tropical cyclone positions and for estimating storm intensities using the method first developed by Dvorak (1972). Furthermore, geostationary sequential satellite imagery can also be used to determine cloud-drift winds, primarily at upper and lower levels (Hubert and Whitney 1971). An obvious limitation of this product resulted from the fact that vast cloud-free regions were left unsampled. Velden *et al*. (1997) developed an algorithm to determine the upper-tropospheric water vapor wind vector (WVWV) fields from GOES-8/9 water vapor observations. Using a variational bogus data assimilation scheme, Zou and Xiao (2000) incorporated the WVWV into the MM5 model to simulate a mature hurricane.

In recent years, products from the passive microwave observations from polar-orbiting satellites have been widely used in the initialization of hurricane models. Microwave observations have two main advantages over visible and infrared observations: (1) microwave radiation penetrates through clouds, and (2) microwave radiation is sensitive to a wide variety of atmospheric parameters, such as atmospheric temperature and moisture, cloud liquid water, cloud ice water, rain, and surface winds.

Krishnamurti et al. (1991) developed a method to physically initialize the FSU Global cumulus parameterization Spectral Model (GSM), which highly depends upon the surface rain rates that were derived from the Special Sensor Microwave Imager (SSM/I). Theoretically, the application of more accurate and consistent rain rates should improve the representation of latent heat release and cumulus parameterization in hurricane models. Krishnamurti et al. (1998) indicated that the intensity forecasts of a hurricane are shown to be quite sensitive to the initial meso-convective scale precipitation distributions. Recently, a comparison study was conducted by Tibbetts et al. (2000) to evaluate the performance of four different rain-rate algorithms in hurricane track forecasts. It was found that the SSM/I rain rate algorithm proves to be the most consistent and accurate rain rate in this study.

Hou et al. (2000a,b) assimilated the TRMM Microwave Imager (TMI) derived surface rainfall and total precipitable water (TPW) into the Goddard Earth Observing System (GEOS) global analysis. A unique feature of the GEOS data assimilation system is that it uses the incremental analysis update (IAU) developed by Bloom et al. (1996), which virtually eliminates the spinup problem. The minimization procedure is one-dimensional, but the evaluation of the cost function involves a 6-h time integration. The procedure minimizes the least squares differences between the observations and the corresponding values generated by the column model averaged over the 6-h analysis window. Pu et al. (2002) used the GEOS global analysis data with and without assimilation of the TMI surface rainfall to study the impact of TRMM surface rain rate on mesoscale numerical simulation of Supertyphoon Paka. It is found that the GEOS analysis can modify the environment of the storm, and the model initial conditions are more favorable for the development of the storm. Consequently, the simulated typhoon structure and intensity is improved significantly. The experiment with

TMI data produces a storm of typhoon intensity after 36 h, while the simulation without TMI data requires 60 h to generate a typhoon.

The satellite microwave sounders directly provide the information on atmospheric temperature and water vapor profiles and their products are demonstrated with greater potentials for uses in the hurricane model initialization. The first Advanced Microwave Sounding Unit (AMSU) instrument on board NOAA 15 satellite was launched in 1998. Since then we have seen many studies to utilize this data in monitoring and simulating tropical cyclones. AMSU measurements can provide much improved information on the atmospheric temperature and moisture profiles, as compared to the Microwave Sounding Unit on earlier NOAA satellites. The associated 3D temperature field has been used to estimate hurricanes' maximum wind (Kidder et al. 2000) and central pressure (Kidder 1978; Velden and Smith 1983; Kidder et al. 2000). In addition, the temperature gradient could be utilized to derive the tangential winds when a hurricane reaches its mature stage with a well-defined circular structure (Grody 1979, Kidder et al. 2000). The above studies demonstrated that AMSU measurements could provide useful information for hurricane modeling. Recently, a new algorithm to construct initial hurricane vortices using the AMSU measurements was developed by Zhu et al. (2002a). In this paper, we are going to test this scheme in more case studies and present some results from the numerical simulate of Hurricane Bonnie (1998).

2. Retrieving hurricane vortices

Zhu et al. (2002a) developed a new algorithm to retrieve three-dimensional temperature, geopotential height, wind, and moisture fields for a hurricane system using the AMSU measurements. There are five procedures to construct a hurricane vortex: (a) retrieving three-dimensional temperature field from AMSU data; (b) integrating hydrostatic equation to obtain geopotential heights; (c) solving the balance equation to obtain the rotational winds; (d) solving the omega equation to obtain the divergent winds; and (e) specifying initial moisture field based on the AMSU-derived total precipitable water. In this section, we will give a brief description of these procedures in the retrieving hurricane vortex for Hurricane Bonnie and test the temperature retrieval algorithm in four tropical cyclones.

2.1. *Retrieving atmospheric temperature*

The AMSU instrument on NOAA-15 satellite contains two modules: A and B. The A module (AMSU-A) has 15 channels and is mainly designed to provide information on atmospheric temperature profiles while the B module (AMSU-B) allows for profiling the moisture field. The instrument has an instantaneous field-of-view of 3.3^{o} and scans $\pm$ 48.3^{o} from nadir with 15 different viewing angles at each side. The AMSU-A measures thermal radiation at microwave frequencies ranging from 23.8 to 89.0 GHz. Atmospheric temperature profiles are primarily based on the measurements obtained at channels (3-14) near 60 GHz, which is an oxygen absorption line. Since the satellite provides a nominal spatial resolution of 48 km at its nadir, the temperature perturbations from synoptic to mesoscale can be reasonably depicted. In addition, several AMSU imaging channels at frequencies of 31.4, 89 and 150 GHz are utilized to determine cloud liquid water and ice water contents because they directly

respond to the thermal emission of liquid droplets and scattering of ice particles (Weng and Grody 2000).

Since microwave radiance responds linearly to temperatures and since the weighting functions at various AMSU sounding channels are relatively stable, temperatures at any pressure level can be expressed as a linear combination of brightness temperatures measured at various sounding channels (see Janssen 1993), i.e.,

$$T(p) = C_0(p,\theta_s) + \sum_{i=1}^{n} C_i(p,\theta_s) T_b(\nu_i,\theta_s) \ , \tag{1}$$

where p is the pressure; θ_s is the scanning angle; ν_i is the frequency at channel i; and T_b is the AMSU brightness temperature. The coefficients, C_0 and C_i, are determined using a regression equation, in the same form as Eq. (1), by matching the rawinsonde temperature soundings with the AMSU-A brightness temperatures that were co-located at islands over the low- to mid-latitude oceans (Zhu et al. 2002a). Two sets of retrieval coefficients are obtained to retrieve temperatures in clear and heavily rainfall regions separately, because the large rain droplets contaminate signals at channels 3 –5. The heavy precipitation region is identified by using the cloud liquid water path (LWP), which is retrieved from the AMSU-A window channels 1 and 2 (Weng et al. 2000).

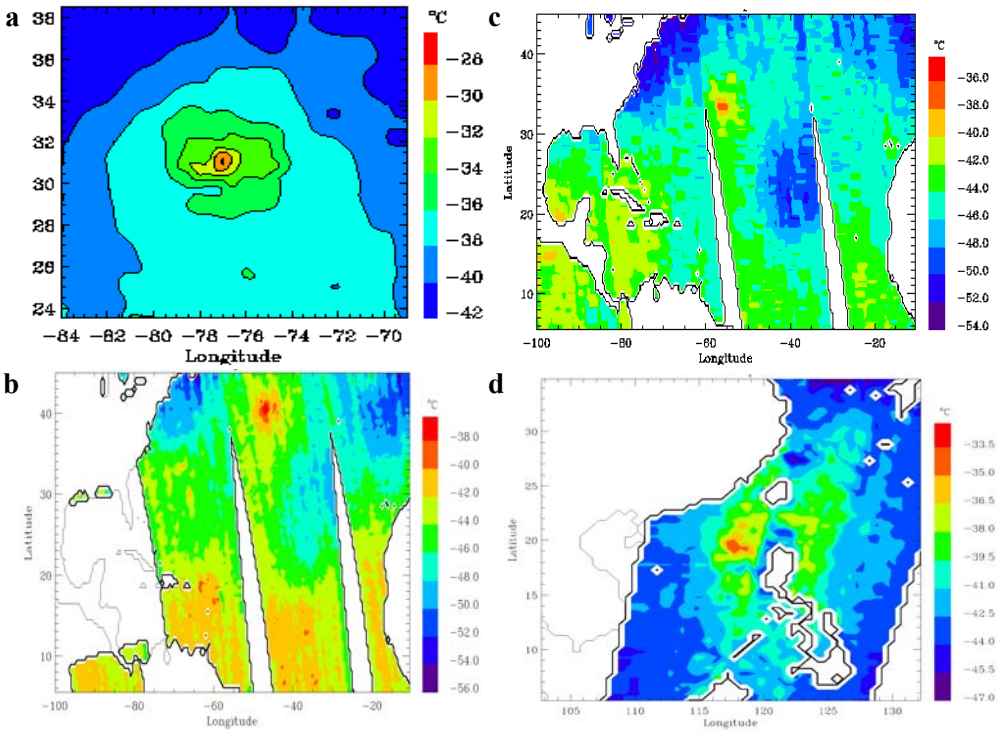

Figure 1. The AMSU-retrieved temperatures at 250 hPa (a) at 0000 UTC 26 Aug 1998 for Hurricane Bonnie, (b) at 2200 UTC 21 Aug 2000 for Hurricane Alberto, (c) at 2200 UTC 29 Sep 2000 for Hurricane Isaac, and (d) at 2300 UTC 05 Oct 1999 for Typhoon Dan.

Four tropical cyclones are studied to examine how the temperature retrieval algorithm performs. Figure 1a shows the retrieved temperature at 250 hPa for Hurricane Bonnie at 0000 UTC 26 Aug 1998. The maximum temperature in the warm core was about -28^{0}C. The temperature anomaly is often defined as a deviation from the unperturbed environmental temperature. Apparently, a warm core of Bonnie can be identified with a maximum for about 10 - 12^{0}C at 250 hPa (Fig. 1a). At this time the minimum sea-level pressure of Bonnie is 958 hPa. Hurricane Alberto (2000) was a long-lived hurricane that remained at sea through its lifetime. At 2200 UTC 21 Aug 2000, it was a Category 2 hurricane with minimum see-level pressure is 975 hPa. Alberto had a warm core of –38^{0}C and the warm temperature anomaly was around 8 – 10^{0}C at 250 hPa (Fig. 1b). Hurricane Isaac (2000) was a Category 3 hurricane at 2200 UTC 29 Sep. 2000 with minimum central pressure of 960 hPa. The retrieved warm core was –38^{0}C and the warm anomaly for about 10^{0}C at 250 hPa (Fig. 1c). We also test the temperature retrieval algorithm for tropical cyclones in the Pacific Ocean. Typhoon Dan had Category 2 intensity with a maximum sustained wind speed of 85 kt at 2300 UTC 05 Oct 1999 in the South China Sea. The AMSU measurements showed an 8^{0}C warm core with –35^{0}C at center over 250-hPa altitude (Fig. 1d). The above results indicate that the AMSU retrieval temperature can depict strong warm core signal at 250-hPa height for tropical cyclones. The magnitude of the retrieved temperature anomaly for each storm is closely related to its intensity in term of the sea-level pressure.

2.2. *Inverting the balanced flow*

After retrieving temperatures from the AMSU data, we are able to obtain the three-dimensional (3D) rotational winds using the balance equation. The gradient balance models have been widely used in theoretical studies of tropical cyclones, and they have provided many fundamental insights into the dynamics of hurricane vortices (Eliassen 1951; Emanuel 1986; Shapiro and Willoughby 1982). The balance equation has also been widely used for initializing primitive equation models as well as for bogusing tropical cyclones (Bolin 1956; Baer 1977). The general form of the balance equation, in terms of geopotential height (ϕ) and stream function (ψ), can be written as

$$f\nabla^2\psi + 2(\psi_{xx}\psi_{yy} - \psi_{xy}^2) + \psi_x f_x + \psi_y f_y = \nabla^2\phi \quad , \tag{2}$$

where f is the Coriolis parameter, and ∇ is the two dimensional (2D) gradient operator. Inverting the stream function from the given geopotential ϕ using the successive over-relaxation (SOR) method is a Monge-Ampere type of problem, in which an ellipticity condition must be satisfied. The inverting procedure includes (a) specifying the sea level pressure distribution using the scheme of Holland (1980); (b) integrating hydrostatic equation using the AMSU-derived temperatures to obtain geopotential heights; (c) solving the stream function from Eq. (2), given the lateral boundary conditions; and (d) calculating horizontal winds from the stream function.

2.3. *Diagnosing the divergent wind component*

It is evident that horizontal winds derived from Eq. (2) are nondivergent. However, there are pronounced vertical motions associated with latent heat release in the eyewall, which should be included as a divergent component in order to alleviate the initial model spin-up problems. The divergent winds could be obtained through vertical velocity diagnosed from the Omega equation, and it is detailed below.

First, the surface rain rates are derived using NOAA's operational AMSU algorithm (Zhao et al. 2001). Second, the vertical distribution of condensational heating must be determined in accordance with the surface rain rates. A normalized latent heating profile is diagnosed from the explicitly simulated Andrew during its mature stage (Liu et al 1997). Third, the divergent wind is obtained, following Tarbell et al. (1981), using the balanced winds and the 3D latent heating field. The following Omega and the continuity equations are employed:

$$\nabla^2(\sigma\omega) + f\zeta_a\frac{\partial^2\omega}{\partial p^2} = f\frac{\partial}{\partial p}(V_\varphi + V_\chi)\cdot\nabla\zeta + \frac{R}{p}(\nabla^2 V_\varphi + \nabla^2 V_\chi)\cdot\nabla T - f\frac{\partial}{\partial p}(\zeta \quad \nabla^2\chi) \tag{3}$$

$$+ f\frac{\partial}{\partial p}(\omega\frac{\partial\zeta}{\partial p}) + f\frac{\partial}{\partial p}(\nabla\omega\cdot\nabla\frac{\partial\varphi}{\partial p}) - \frac{R}{C_p P}\nabla^2 Q,$$

$$\nabla^2\chi + \frac{\partial\omega}{\partial p} = 0, \tag{4}$$

where $\sigma \equiv -\frac{RT}{p\theta}\frac{\partial\theta}{\partial p}$ is the static stability and Q is the diabatic heating rate. An iterative procedure is required to solve ω and V_χ from Eq. (3) and (4). Since the latent heating is a major forcing term in the Omega equation, we do see the convergence (divergence) of the lower- (upper-) level flows in the rainfall regions with the divergent winds at about ± 5 m s^{-1} after the above procedure.

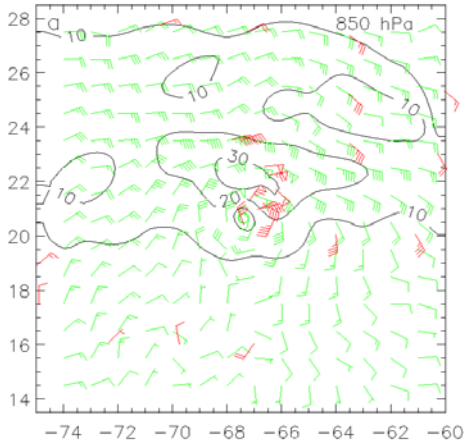

Figure 2. The horizontal winds retrieved from the AMSU (in green) and obtained from the GPS dropsonde measurements (in red) at 0000 UTC 22 August 1998. Solid lines are isotaches at intervals of 5 m s^{-1}. The storm center is denoted by a green hurricane symbol (after Zhu et al. 2002a).

After obtaining the divergent winds, the total horizontal winds are just the sum of the rotational and divergent winds. Figure 2 shows the retrieved total flows at 850 hPa at 0000 UTC 22 Aug 1998 when Bonnie reached Category 1 hurricane intensity. At this time, there were global positioning system (GPS) dropsondes available to provide verification. In general, the retrieved winds agree with the observed at 850 hPa in both speed and direction. Since the GPS dropsonde data near the storm center were measured around 2130 UTC 21 August, and the satellite passed the spot at 0000 UTC 22 August, the retrieved vortex center is located on the west of the observed by about 0.5^0. The retrieved maximum wind is 32 m s^{-1}, in good agreement with the observed. Both the retrieved and observed winds show a region in excess of 30 m s^{-1} on the north of the storm center; whereas on the south winds are relatively weak.

3. Simulation of Hurricane Bonnie

Using the above derived initial hurricane vortex at 0000 UTC 22 Aug 1998, we perform a 5-day simulation of Hurricane Bonnie and analyze Bonnie's inner-core structures in this section. The hurricane-scale moisture and SST fields for model initial and boundary conditions are also specified according to satellite microwave measurements.

3.1. *A 5-day simulation of Bonnie*

Hurricane Bonnie is the first major hurricane that took place in the Atlantic Ocean shortly after the launch of the National Oceanic and Atmospheric Administration-15 (NOAA-15) satellite with the AMSU instrument on board. Bonnie exhibited two interesting characters that were distinct from other hurricanes (e.g., Andrew in 1992) during its life span. The first one is the evolution of storm intensity showing a rapid deepening for a two-day period after reaching Category 1 on 22 August 1998, followed by a near-steady state over the open ocean during the next three days (i.e., 24-27 August). The second distinct character is the evolution of precipitation in the eyewall, i.e., from a partial to near-concentric eyewall during 22-27 August. In this section, we will present some interesting features associated with the asymmetric eyewall structures in the simulated storm.

Hurricane Bonnie (1998) is explicitly simulated using the PSU/NCAR nonhydrostatic, two-way interactive, movable, triply nested grid model (i.e., MM5V3.4, Dudhia 1993 and Grell et al. 1995) with the finest mesh grid length of 4 km. The model physics used include the Goddard cloud microphysics scheme (Tao and Simpson, 1993; Simpson and Tao 1993), the Kain-Fritsch (1993) convective parameterization scheme, the Blackadar PBL scheme (Zhang and Anthes 1982) and a cloud-radiation interaction scheme, which are similar to those given in Liu et al. (1997). Although no convective parameterization is applied over the finest mesh, a shallow convective scheme is used. There are 24 σ levels or 23 half-σ layers in the vertical, which is the same as that used by Liu et al. (1997). A 5-day simulation is performed, covering the initial rapid deepening, steady variation and landfalling stages of the storm. See Zhu et al. (2002a,b) for detailed model design.

The model initial conditions and lateral boundary conditions are obtained from the National Centers for Environmental Prediction (NCEP) 2.5^0 x 2.5^0 global analysis, which is then enhanced by rawinsondes and surface observations. Because the NCEP analysis contains a vortex with a central pressure of 12 hPa weaker than the observed, the above derived hurricane vortex is incorporated into the model initial conditions. The initial moisture field in NCEP analysis is also too dry, particularly in the hurricane eyewall regions. Thus, we iteratively retrieve the 3D moisture field using the Total Precipitable Water (TPW) retrieved from AMSU-A measurements (Grody et al. 2001) as a constraint. The simulated mean RH profiles given in Liu et al. (1999) are used here as a reference to set the maximum and minimum RH values in the vertical. The iteration starts from the minimum RH value at a given point, and then computes TPW by vertically integrating its associated specific humidity. The difference between the new TPW and the satellite-retrieved TPW is used to compute a new RH profile. At most points, the calculated TPW values could converge to the satellite-retrieved within 50 iterations.

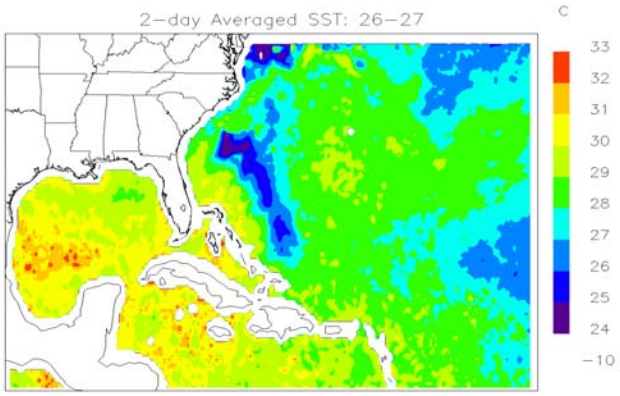

Figure 3. The 2-day averaged SST obtained by Tropical Rainfall Measuring Mission (TRMM) Microwave Imager (TMI) for the period from 0000 UTC 26 to 0000 UTC 27 Aug 1998.

Since this is a 5-day simulation, the oceanic feedback becomes an important factor influencing the intensity of the storm. For this reason, the SST is updated daily using the Tropical Rainfall Measuring Mission (TRMM) Microwave Imager (TMI) Level-1 standard product at 0.25^0 x 0.25^0 Lat/Lon resolution (Chelton et al. 2000). Although the TRMM/TMI SST can be measured underneath clouds, there are still some missing data near the storm center due to the contamination by heavy rain droplets. They are filled by a three-day running mean of SST at each grid point. A 2-day averaged SST is given in Fig. 3, which shows more than 4^0C SST cooling along and to the north of Bonnie's track. It can be seen that the cold SST maintained for about 2 days after the storm passed. According to our sensitivity test to be shown in a forthcoming paper and the coupled ocean-atmosphere model simulations of Hong et al. (2000), this SST cooling could account for about 20-hPa central pressure changes in simulations with or without the SST feedback.

3.2. *Simulation results*

The simulated track compares favorably to the observed (not shown), which shows similar paths in the first 12 h. Then, Bonnie changed its tracking direction from west-northwest to northwest, whereas the simulated one keeps moving west-northwestward. The simulated track deviates from the observed by about 200 km at 24 h. After 48 h, the simulated storm moves closer to the best track, but still with a distance error of 250 km, and it also re-curves somewhat earlier than the observed at 84 h. The simulated landfall occurs to the northeast of the observed by about 150 km and 20 h earlier.

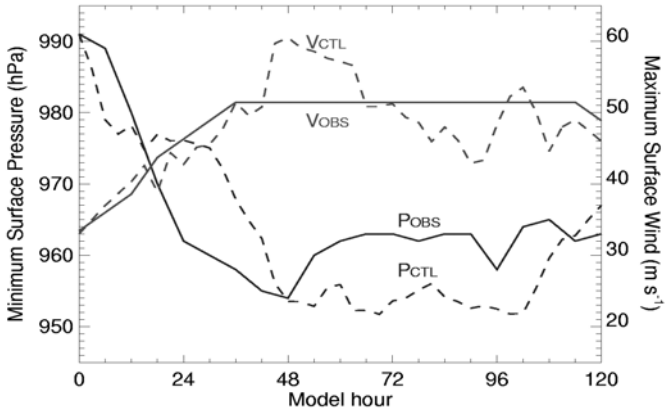

Figure 4. Time series (6 hourly) of the minimum central pressures (P in hPa) and the maximum surface winds (V in m s^{-1}) from the best analysis (solid, P_{OBS} and V_{OBS}) and the model simulation (dashed, P_{CTL} and V_{CTL}) (after Zhu et al. 2002b).

Figure 4 compares the simulated hurricane intensity to the observed. They are in general agreement but differ in details during the 5-day period. Initially, the modeled storm (P_{CTL}) deepens more rapidly than the observed (P_{OBS}), indicating the absence of the model spin-up problem. However, the model storm experiences a slow deepening period from 12 to 30 h. This is likely caused by the presence of a too dry environment that fails to feed the needed energy in the PBL inflow for the continued deepening, since the initial moisture field outside of the hurricane vortex was not modified in the model initial conditions. A deepening rate, similar to the observed, does not occur until the 30-h simulation when the model storm begins to receive comparable energy supply through the air-sea interaction processes. The simulated storm reaches the minimum central pressure of 954 hPa as the observed at 48 h, and maintains its intensity with weak oscillations afterwards. During the maintenance stage, the simulated storm is about 6-8 hPa deeper than the observed. Part of this difference could clearly be attributed to the fact that the simulated storm moves to the southwest of the best track in the first 3 days where local SST is about 1 to 2^0 warmer than that to its north. Nevertheless, the two distinct development stages of rapid deepening and slow maintenance are considered being reasonably reproduced. The simulated maximum surface winds (V_{CTL})

also compare favorably to the observed (V_{OBS}). The two distinct development stages could also be seen from both the simulated and observed wind fields.

3.3. *Diagnoses of partial eyewall feature*

The simulated radar reflectivity from the 46-h control simulation is calculated, following Liu et al. (1997), which exhibits highly asymmetric structures of the eyewall and cloud bands (Fig. 5). Specifically, the model produces a partial eyewall in the east and an organized rainband spiraled outward in the northeast semicircle. Of interest is that much weaker or little convective activity occurs on the west, which is in significant contrast with the simulated Hurricane Andrew (1992) shown in Liu et al. (1997). The simulated structures compare favorably to the radar observations by NOAA's WP-3D aircraft during the Convective and Moisture Experiment-3 (CAMEX-3), including the general location, size, and intensity of the eyewall/rainband, although the observed location is about 200 km to the northeast.

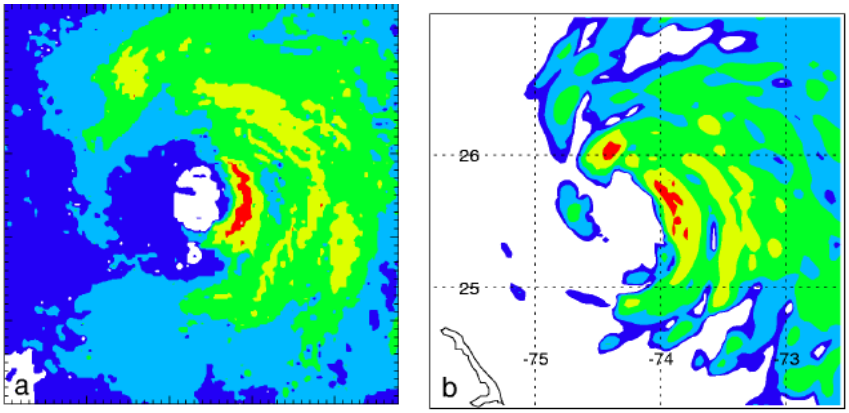

Figure 5. Radar reflectivity (at 15, 21, 28, 35, 41 and 48 dBZ) from (a) NOAA's WP-3D reconnaissance aircraft at 2130 UTC 23 August at the 4544-m altitude; (b) the control simulation at 2200 UTC 23 August near 480 hPa. The two panels have the same color scale and the same domain size of 360 km x 360 km (adapted from Zhu et al 2002a).

Many earlier observations have shown the presence of asymmetric clouds, precipitation and winds in tropical cyclones. The downshear-left asymmetric eyewall pattern has also been clearly demonstrated by idealized model simulations. Frank and Ritchie (1999) simulated tropical-cyclone-like vortices under different vertical wind shear environments using the MM5 model. They found that more intense convection tends to be organized at the left side of the shear vector, looking downshear. There are several hypotheses for the relationship between vertical shear and hurricane asymmetries. These hypotheses all emphasize the processes in lower atmospheric layers, such as the frictional drag (Shapiro 1983), and the low-level convergence and divergence (Willoughby et al. 1984, Bender 1997). In the next, we examine the influence of vertical wind shears on the development of the partial eyewall and other related inner-core structures using the simulation results for Hurricane Bonnie.

Figure 6 presents a few selected trajectories from 42 – 54 h using 15-minutes model output in order to see the extent of vertical and horizontal displacements associated with the descending and ascending motion in western and eastern eyewall, respectively. The first group of seeds is put in the west eyewall at the altitude of 9 km. The backward trajectory indicates that the air parcels come from the upper-level jet flow region northwest of the storm at about 12-km height. After reaching the west eyewall region, this flow converges and goes downward to 9-km height, then circles cyclonically from the west quadrant to the south quadrant. Once the flow goes out of the eyewall at the south quadrant, it climbed up to 13 km gradually. The second group of seeds is released around 7-km altitude in the west eyewall. This flow comes from the northeast side of environmental region, and it goes into the eyewall at northwest quadrant at 9 km altitude. It takes about 3 h for the flow to complete a half circle in the western eyewall at a speed for about 25 m s^{-1}, and then goes out of the eyewall at the southeast quadrant. Once outside the eyewall, the flow slows down and climbs to 13 km eventually. By examining the low-level trajectories, it is found that there are two sources of moist air that converge into the east eyewall from the southwest and the southeast environmental regions. The air parcels climb from 100 m to 3.5 km when it first reaches the east eyewall. After one circle, the flow reaches 6 km altitude in the eastern eyewall.

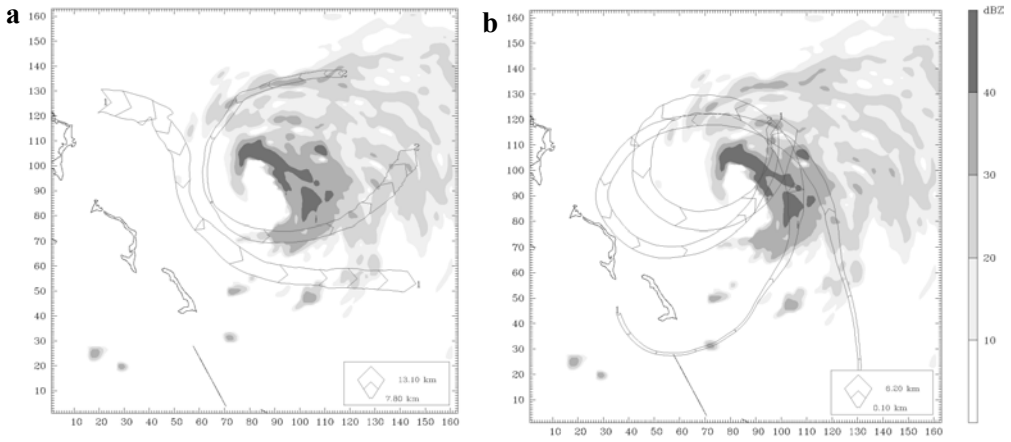

Figure 6. The 6 hourly backward and forward trajectories for parcels released at 48-h simulation (i.e., 0000 UTC 24 August). (a) Number 1 and 2 parcels are released in the western eyewall at z = 9 and 7 km, respectively, (b) Number 3 and 4 parcels are released in the eastern eyewall at z = 3.5 km. Radar reflectivity at σ = 0.44 level is shaded at intervals of 10 dBZ. A trajectory is shown as a curved ribbon, with its width proportional to the height of the trajectory. The arrowheads are drawn along each trajectory at 1-h intervals.

The above trajectory analysis indicates that an upper-level westerly flow enters the eyewall with a deeper and stronger inflow in the northwest. Because the environmental air is clod and dry, downdrafts are initiated in the inflow region, with the significant enhancement from evaporative cooling. The dry descent causes the adiabatic warming and drying in the middle-level, and stabilizes the atmosphere at the west part of eyewall. Therefore the

developments of clouds and precipitation in the western eyewall are suppressed and the partial eyewall feature is generated.

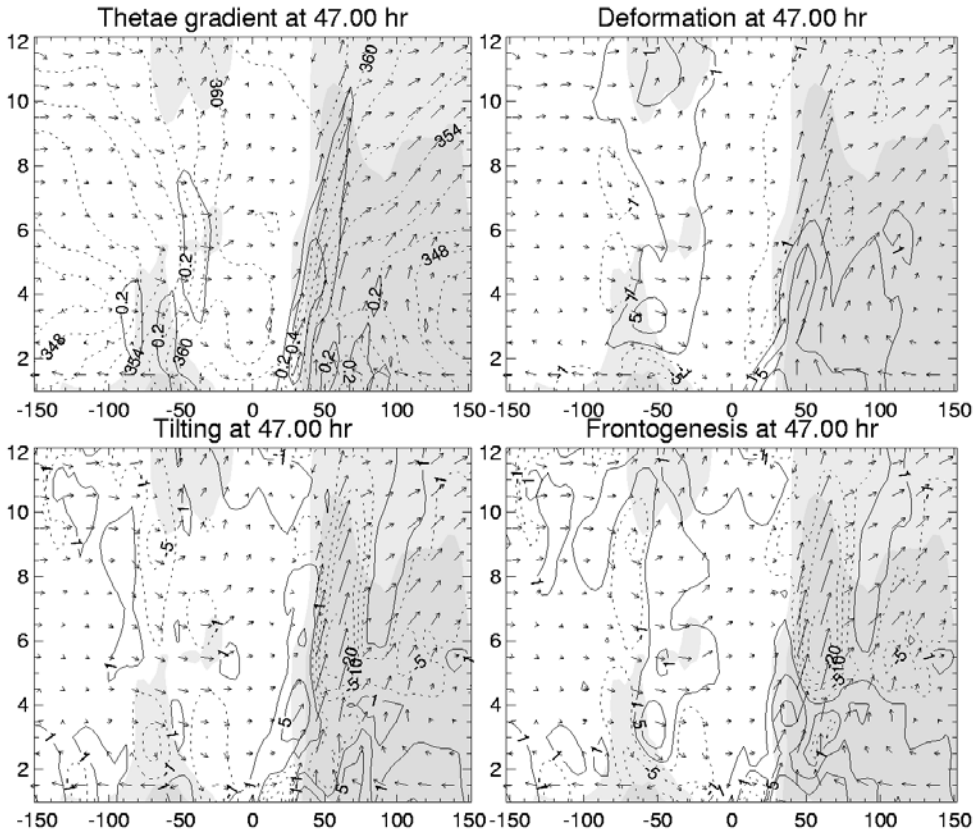

Figure 7. West-east vertical cross sections through the minimum pressure center of (a) potential temperature (dashed) and its gradient (solid); and (b) frontogenesis due to the deformation term; (c) frontogenesis due to the tilting term; and (d) total frontogenesis for the averaged period from 46 to 47 h. Radar reflectivity is shaded at 15 and 30 dBZ. In-plane flow vectors are also superposed.

Finally, the frontogenesis function is computed to examine the formation of the partial eyewall feature from kinematic considerations. The frontogenesis function has been widely used to investigate mid-latitude frontogenesis and cyclogenesis (Miller, 1948; Bosart, 1970; Baldwin et al., 1984; Lapenta and Seaman 1990; Doyle and Warner 1993). Emanuel (1997) pointed out that the hurricane eyewall is not necessarily a front in surface temperature, but instead involves the equivalent potential temperature (θ_e) distribution, which is directly related to density in saturated air. At 47 h, the strong warm anomaly or the strong gradient of potential temperature (θ) is located at the west side of eyewall because of the subsidence warming, while there is little deep convection. However, the $|\nabla_H \theta_e|$ is weak at the west and strong at the east sides of eyewall (Fig. 7a). This asymmetric pattern is similar to that of radar reflectivity. In order to focus on the asymmetric convection feature, we will analyze the

frontogenesis in term of θ_e instead of θ. The temporal rate change of the gradient of θ_e following a parcel is defined as the same as that in Lapenta and Seaman (1990) except for the replacement of θ by θ_e and therefore the absence of the condensation term,

$$\frac{d}{dt}|\nabla_H\theta_e| = -|\nabla_H\theta_e|^{-1}\left\{\left[\left(\frac{\partial\theta_e}{\partial x}\right)^2\frac{\partial u}{\partial x}+\left(\frac{\partial\theta_e}{\partial y}\right)^2\frac{\partial v}{\partial y}\right]+\left[\frac{\partial\theta_e}{\partial x}\frac{\partial\theta_e}{\partial y}\left(\frac{\partial v}{\partial x}+\frac{\partial u}{\partial y}\right)\right]\right\} - |\nabla_H\theta_e|^{-1}\left[\left(\frac{\partial\theta_e}{\partial x}\frac{\partial\theta_e}{\partial z}\right)\frac{\partial w}{\partial x}+\left(\frac{\partial\theta_e}{\partial y}\frac{\partial\theta_e}{\partial z}\right)\frac{\partial w}{\partial y}\right], \quad (5)$$

where ∇_H is the horizontal gradient operator. The first term on the right-hand side of Eq. (5) represents the contribution of the deformation field to the frontogenesis, including the horizontal confluence and shearing effect. The second term is the contribution from twisting or tilting effect. Note that there is no surface friction term in Eq. (5), because we will focus our attention above the maritime boundary layer, especially the middle and upper troposphere where the significant asymmetries occur.

In this analysis, a one hour averaged dataset is used, which is obtained from a 10-min interval dataset for the period from 46 to 47 h. This is the time when the storm already has asymmetric structures. The typical value of total frontogenesis is approximately 1 K $(1\ km)^{-1}$ $(1\ day)^{-1}$ in our analysis, and is about 50 times larger than that in coastal frontogenesis (Lapenta and Seaman 1990; Doyle and Warner 1993). It is mainly because the magnitudes of the variables in hurricane system are larger than that in the mid-latitude front system, and our model resolution is higher.

The west-east vertical cross section of $|\nabla_H\theta_e|$, the deformation term, the tilting term and the total frontogenesis through hurricane eye are shown in Fig. 7. The frontogenesis function due to the deformation term is positive at the lower and middle levels of the east side of the storm and the middle and upper levels of the west side of the storm (Fig. 7b), as a result of the convergence of environmental flow. The effect of the deformation term is frontolytic at the low level in the west eyewall and upper level in the east eyewall, associated with the diffluence zone. The contribution by the tilting term is strong at where there is strong vertical motion. At the west side of the eyewall, there are two frontolytic regions at lower and upper levels as a result of the tilting term (Fig. 7c). A deep frontolytic layer exists in the east side of the eyewall, with the maximum at middle and upper levels. A strong frontogenetic zone is produced immediately inside the east eyewall by the tilting term. Overall, the total frontogenesis function (Fig. 7d) is frontolytic in the west eyewall, with the contributions from deformation term at the low level and tilting term at the middle and upper levels. Right inside the west eyewall, there is frontogenetic region at the middle and upper levels, mainly as a result of the confluent flow from the upper level. To the east of the center, strong frontogenesis is produced immediately inside the old eyewall with the positive contributions from both deformation and tilting terms. The strong frontolytic zone is created in the eyewall above 5 km by the tilting term. The effects of the west side frontolytic zone, especially in the low level eyewall, will continue to reduce the convections in that region. The total

frontogenesis developed inside the east and west eyewalls (around 40-50 km region) suggests that the radius of the inner eyewall is going to keep decreasing. The frontogenesis develops at the eastern side for about 80 km area indicates that an outer rainband is going to form there.

4. Summary and conclusions

Tropical cyclones develop over the ocean, where few traditional rawinsonde observations are available. Satellite observations have been proved as the most useful data source for tropical cyclone monitoring and forecasting. In this paper, we reviewed several satellite products and the methods to incorporate them into numerical models to improve hurricane forecasts. Because microwave radiation penetrates through clouds and is sensitive to a wide variety of atmospheric parameters, satellite microwave observations, such as AMSU data, are extremely useful in the study of tropical cyclones.

Four tropical cyclones are studied to examine the general capability of a newly developed AMSU temperature retrieval algorithm. It is found that the retrieved temperature can depict a strong warm core at 250-hPa height for tropical cyclones. The magnitude of the retrieved temperature anomaly for each storm is closely related to its intensity in term of sea-level pressure. The geopotential heights are calculated by integrating hydrostatic equation from the bottom upward with the retrieved temperatures. The asymmetric vortex flows are attained by solving the nonlinear balance equation, using the NCEP analysis as the lateral boundary conditions. The divergent wind component is obtained by solving the Omega equation, in which the latent heating profile is specified with the magnitude based on the AMSU-A surface rain rate and the vertical structure based on the previously simulated hurricane. The retrieved temperature and wind fields associated with Hurricane Bonnie compare favorably to the GPS dropsonde observations during CAMEX-3.

Using the above derived initial hurricane vortex, a 5-day simulation of Hurricane Bonnie (1998) is performed with triply nested mesh and the finest grid size of 4 km. The model initial moisture field of the hurricane vortex is derived from the AMSU-derived TPW, assuming that RH is constant in the eyewall cloud regions. During the model integration, the SST is updated daily according to the TRMM/TMI observation. The simulated track is within 3 degree lat/lon of the best-track during the 5-day integration, with the landfalling point close to the observed. The model also reproduces the hurricane intensity changes during the 5-day period, including the deepening and maintaining stages. The simulated radar reflectivity shows pronounced asymmetries in the eyewall and rainbands around 45 h, in agreement with the observations from WP-3D radar.

Trajectory analyses indicate that the upper-level westerly flow converges into the west eyewall, and then descends and cyclonically circles around the center from the west to the south sector. The cyclonic flow at middle and lower levels in the eyewall was also forced downward in the west to south quadrant. Because of the strong descending motion, the warm core shifted to the west. The mid-level warming stabilizes the atmosphere at the west part of eyewall, and the convections are confined at low-levels. When the storm develops the partial eyewall feature, the frontogenesis function is frontolytic in the west eyewall, with the

contributions from deformation term at the low level and from tilting term at the middle and upper levels. It is found that the upper-level strong inflow is a key factor that leads to the development of the partial eyewall.

Acknowledgments. This work was supported by NOAA/NESDIS, NSF Grant ATM-9802391, and NASA Grant NAG-57842. The first author wishes to express profound gratitude to his dissertation advisor Dr. Da-Lin Zhang for giving a lot of guidance throughout this study. We want to thank Ms. Huan Meng at NOAA/NESDIS/ORA for helping us to obtain AMSU data. We would also like to thank scientists at Hurricane Research Division/AOML/NOAA and NASA Goddard Space Flight Center for providing the CAMEX-3 observations through their websites.

References:

Baer, F., 1977: The spectral balance equation. *Tellus,* **29,** 107-115.

Baldwin, D., E.-Y., Hsie, and R. A. Anthes, 1984: Diagnostic studies of a two-dimensional simulation of frontogenesis in a moist atmosphere. *J. Atmos. Sci.*, **41**, 2686-2700.

Bender, M., 1997: The effect of relative flow on the asymmetric structure in the interior of hurricanes. *J. Atmos. Sci.*, **54**, 703-724.

Bloom, S. C., L. L. Takacs, A. M. da Silva, and D. V. Ledvina, 1996: Data assimilation using incremental analysis updates. *Mon. Wea. Rev.,* **124**, 1256–1271.

Bolin, B., 1956: An improved barotropic model and some aspects of using the balance equation for three-dimensional flow. *Tellus*, **8**, 61-75.

Bosart, L. F., 1970: Midtropospheric frontogenesis. *Quart J. Roy. Meteor. Soc.*, **96**, 442-471.

Chelton, D.B., F.J. Wentz, C.L. Gentemann, R.A. de Szoeke, and M.G. Schlax, 2000: Satellite microwave SST observations of transequatorial tropical instability waves. *Geophys. Res. Letters*, **27**, 1239-1242.

Doyle, D. J., and T. T. Warner, 1993: A numerical investigation of coastal frontogenesis and mesoscale cyclogenesis during GALE IOP 2. *Mon. Wea. Rev.*, **121**, 1048-1077.

Dudhia, J., 1993: A nonhydrostatic version of the Penn State-NCAR mesoscale model: Validation tests and simulation of an Atlantic cyclone and cold front. *Mon. Wea. Rev.,* **121,** 1493-1513.

Dvorak, V. F., 1972: A technique for the analysis and forecasting of tropical cyclone intensities from satellite pictures. NOAA TMNESS 36, U.S. Dept. of Commerce, Washington, DC, 15 pp.

Eliassen, A., 1951: Slow thermally or frictionally controlled meridional circulation in a circular vortex. *Astrophys. Norv*., **5,** 19-60.

Emanuel, K. A., 1986: An air-sea interaction theory for tropical cyclone. Part I: Steady-state maintenance. *J. Atmos. Sci.,* **43,** 585-604.

___, 1997: Some aspects of hurricane inner-core dynamics and energetics. *J. Atmos. Sci.*, **54**, 1014-1026.

Frank, W. M., and E. A. Ritchie, 1999: Effects of environmental flow upon tropical cyclone structure. *Mon. Wea. Rev.,* **127,** 2044-2061.

Grell, G. A., J. Dudhia, and D. R. Stauffer, 1995: A description of the fifth generation Penn State/NCAR mesoscale model (MM5). NCAR Tech Note NCAR/TN-398+STR, 138 pp. [Available from NCAR Publications Office, P. O. Box 3000, Boulder, CO 80307-3000.]

Grody, N., C., 1979: Typhoon "June" winds estimated from scanning microwave spectrometer measurements at 55.45 Ghz. *J. Geophys. Res.*, **84**, 3689-3695.

_____, J. Zhao, R. Ferraro, F. Weng and R. Boers, 2001: Determination of precipitable water and cloud liquid water over oceans from the NOAA-15 Advanced Microwave Sounding Unit (AMSU). *J. of Geophys. Res.,* **106**, 2,943-2,953.

Holland, G. J., 1980:An analytic model of wind and pressure profiles in hurricanes. *Mon. Wea. Rev.*, **108**, 1212-1218.

Hong, X., S. W. Chang, S. Raman, L. K. Shay, and R. Hodur, 2000: The Interaction between Hurricane Opal (1995) and a warm core ring in the Gulf of Mexico. *Mon. Wea. Rev.*, **128**, 1347-1365.

Hou, A. Y., D. V. Ledvina, A. M. Da Silva, S. Q. Zhang, J. Joiner, and R. M. Atlas, 2000a: Assimilation of SSM/I-derived surface rainfall and total precipitable water for improving the GEOS analysis for climate studies. *Mon. Wea. Rev.,* **128**, 509–537.

_____, S. Q. Zhang, A. M. Da Silva, and W. S. Olson, 2000b: Improving assimilated global datasets using TMI rainfall and columnar moisture observations. *J. Climate.,* **13**, 4180–4195.

Hubert, L. F., and L. F. Whitney Jr., 1971: Wind estimation from geostationary satellite pictures. *Mon. Wea. Rev.,* **99,** 665-672.

Janssen, M. A., 1993: *Atmospheric Remote Sensing by Microwave Radiometry*. Wiley Seies in Remote Sensing, John Wiley & Sons, Inc., 572pp.

Kain, J. S., and J. M. Fritsch, 1993: Convective parameterization for mesoscale models: The Kain-Fritsch scheme. *The Representation of Cumulus Convection in Numerical Models, Meteor. Monogr.,* No. 46, Amer. Meteor. Soc., 165–170.

Kidder, S. Q., W. M. Gray, and T.H. Vonder Harr, 1978: Estimating tropical cyclone central pressure and outer winds from satellite microwave data. *Mon. Wea. Rev.*,**108**, 144-152.

_____, M. D. Goldberg, R. M. Zehr, M. DeMaria, J. F. W. Purdom, C. S. Velden, N. C. Grody, and S. J. Kusselson, 2000: Satellite analysis of tropical cyclones using the advanced microwave sounding unit (AMSU). *Bull. Amer. Meteor. Soc*. **81,** 1241-1260.

Krishnamurti T. N., Xue J., Bedi H. S., Ingles K., and D. Oosterhof, (1991): Physical initialization for numerical weather prediction over the tropics. *Tellus*, **43**, 53-81.

_____, Han W., and D. Oosterhof, (1998): Sensitivity of hurricane intensity forecasts to physical initialization. *Meteorol. Atmos. Phys*., **65**, 171-181.

Lapenta, W. M., and N. L. Seaman, 1990: A numerical investigation of east coast cyclogenesis during the cold-air damming event of 27-28 February 1982. Part I: Dynamic and thermodynamic structure. *Mon. Wea. Rev.*, **118**, 2668-2695.

Liu, Y., D.-L. Zhang, and M. K. Yau,1997: A multiscale numerical study of Hurricane Andrew(1992). Part I: Explicit simulation and verification. *Mon. Wea. Rev*., **125**, 3073-3093.

——, ——, and ——,1999: A multiscale numerical study of Hurricane Andrew(1992). Part II: Kinematics and inner-core structures. *Mon. Wea. Rev*., **127**, 2597-2616.

Miller, J. E., 1948: On the concept of frontogenesis. *J. Meteor.*, **5**, 169-171.

Pu, Z.-X., W.-K. Tao, S. Braun, J. Simpson, Y. Jia, J. Halverson, W. Olson, and A. Hou, 2002: The impact of TRMM data on mesoscale numerical simulation of Supertyphoon Paka. *Mon. Wea. Rev.,* **130**, 2448-2458.

Shapiro, L. J., and H. E. Willoughby, 1982: The response of the balance hurricanes to local sources of heat and momentum. *J. Atmos. Sci.,* **39,** 378-394.

_____, 1983: Asymmetric boundary layer flow under a translating hurricane. *J. Atmos. Sci.*, **40**, 1984-1998.

Simpson, J., and W.-K. Tao, 1993: The Goddard Cumulus Ensemble Model. Part II: Applications for studying cloud precipitating processes and for NASA TRMM. *Terr. Atmos. Oceanic Sci.,* **4**, 73–116.

Tao, W.-K., and J. Simpson, 1993: the Goddard cumulus ensemble model. Part I: Model description. *Terr. Atmos. Oceanic Sci.,* **4,** 35-72.

Tarbell, T. C., T. T. Warner, and R. A. Anthes, 1981: An example of the initialization of the divergent wind component in a mesoscale numerical weather prediction model. *Mon. Wea. Rev*., **109**, 77-95.

Tibbetts, R. T., and T. N. Krishnamurti, 2000: An intercomparison of hurricane forecasts using SSM/I and TRMM rain rate algorithm(s). *Meteor. Atmos. Phys.,* **74,** 37-49.

Velden, C. S., and W. L. Smith, 1983: Monitoring tropical cyclone evolution with NOAA satellite microwave observation. *J. Climate Appl. Meteor*., **22**, 714-724.

_____, C. M. Hayden, S. J. Nieman, W. P. Menzel, and S. T. Wanzong, 1997: Upper-tropospheric winds derived from geostationary satellite water vapor observations. *Bull. Amer. Meteor. Soc.,* **78**, 173-195.

Weng, F., and N. C. Grody, 2000: Retrieval of ice cloud parameters using a microwave imaging radiometer, *J. Atmos. Sci.*, 57, 1069-1081.

_____, R. R. Ferraro, and N. C. Grody, 2000: Effects of AMSU cross-scan asymmetry of brightness temperatures on retrieval of atmospheric and surface parameters. *Microwave Radiometry & Remote Sensing of theEarth's Surface and Atmosphere,* Ed. P. Pampaloni and S. Paloscia, VSP, Netherlands, 255-262.

Willoughby, H. E., F. D. Marks, and R. J. Feinberg, 1984: Stationary and moving convective bands in hurricanes. *J. Atmos. Sci.*, **41**, 3189-3211.

Zhang, D.-L. and R. A. Anthes, 1982: A high-resolution model of the planetary boundary layer – sensitivity tests and comparisons with SESAME-79 data. *J. Appl. Meteor.,* **21,** 1594-1609.

Zhao, L., F. Weng, and R.R. Ferraro, 2001: A phasically-based algorithm to derive cloud and precipitation parameters using AMSU measurements, *Preprints, 11th Satellite Conf. on Meteor. & Oceano.,* Amer. Meteor. Soc., Madison, in press.

Zhu, Tong, D.-L. Zhang, and F. Weng, 2002a: Impact of the advanced microwave sounding unit measurements on hurricane prediction. *Mon. Wea. Rev.* **130**, 2416-2432.

_____, _____, _____, 2002b: Numerical Simulation of Hurricane Bonnie (1998). Part I: Eyewall Evolution and Intensity Changes. Submit to *Mon. Wea. Rev.*

Zou, X., and Q. Xiao, 2000: Studies on the initialization and simulation of a mature hurricane using a variational bogus data assimilation scheme. *J. Atmos. Sci.,* **57,** 836-860.